RMetS
Royal Meteorological Society

Impact of surface characteristics on flow over a mesoscale mountain

Marius O. Jonassen,[a]* Hálfdán Ágústsson[b,c] and Haraldur Ólafsson[a,b]
[a]*Bergen School of Meteorology, Geophysical Institute, University of Bergen, Norway*
[b]*Department of Physics, University of Iceland and Icelandic Meteorological Office, Reykjavík, Iceland*
[c]*Institute for Meteorological Research, Reykjavík, Iceland*

*Correspondence to: M. O. Jonassen, Geophysical Institute, University of Bergen, Allégaten 70, 5007 Bergen, Norway.
E-mail: marius.jonassen@gfi.uib.no

Dynamical downscaling of atmospheric flow over Iceland has revealed that prominent downslope accelerated flows are not merely extreme events, but rather constitute a strong climatological signal over the larger ice caps. Ice caps are characterised by smooth and cold surfaces and both of these properties have previously been found to enhance downslope flows. In this article, we investigate the response of downslope accelerated flow over Hofsjökull in Central Iceland to an increase in surface roughness and a change in surface temperature corresponding to the effect of melting Hofsjökull's ice cap. We do so by exploring the flow over Hofsjökull for a summertime case by means of several numerical sensitivity experiments. In the experiments, we find a stronger downslope flow acceleration with than without the ice cap. While an increased surface roughness distinctly dampens the downslope flow, the effect of changing the surface temperature is minimal. This study is both of general relevance through its exploration of factors affecting downslope acceleration of stably stratified flow and also of interest because glaciers diminish rapidly in a changing climate.

Key Words: gravity waves; downslope winds; surface roughness; surface heating; Iceland

Received 26 July 2012; Revised 8 November 2013; Accepted 15 November 2013; Published online in Wiley Online Library 12 February 2014

1. Introduction

Several investigations have revealed a damping effect of surface friction on mountain waves and downslope flow acceleration (e.g. Richard *et al.*, 1989; Georgelin *et al.*, 1994; Ólafsson and Bougeault, 1997a; Epifanio and Qian, 2008). The suppressing effect of surface friction on waves in real flows has also been confirmed for a collection of flows during the PYREX campaign (Ólafsson and Bougeault, 1997b) and subsequently for several individual cases of downslope flow. Peng and Thompson (2003) hypothesized that the reduction in mountain-wave amplitude and drag in the presence of surface friction is due to the reduction in the slope of the atmospheric boundary-layer (ABL) height compared with the terrain height, which is based on the comprehensive standpoint of viewing separately the ABL and the stratified layer above.

Among the first to document analytically the effect of surface heat fluxes on mountain flow was Raymond (1972), who solved a diabatic form of Long's equation. He found surface heating to have a damping effect on mountain waves and surface cooling to have the inverse effect. These results are in line with newer studies using 2D idealised simulations, such as that by Smith and Skyllingstad (2009) who studied the effect of surface heat fluxes on internal gravity wave (IGW) breaking and downslope flows. Using a similar numerical set-up to Smith and Skyllingstad (2009), Smith and Skyllingstad (2011) studied the impact of surface heating and cooling on downslope flows in the presence of a strong elevated inversion. They found that surface cooling in conjunction with a low-level inversion, where strong downslope flow can be attributed to a shallow-water transition rather than IGW breaking, facilitated the generation of strong downslope flows. Surface heating, on the other hand, was found to reduce the low-level inversion strength or change the wind velocity and stratification below the inversion which in turn prevented the downslope windstorm. Furthermore, Smith and Skyllingstad (2011) found a significant contribution from drainage flow in the acceleration of the flow far downstream when a strong low-level inversion was present. For a higher inversion, the katabatic contribution was minimal anywhere in the downstream jet. These simulations support the work of Vosper (2004) on low-level inversions and downslope accelerated flow. The results on surface heating and cooling and the presence of strong low-level inversions are in agreement with downslope windstorms being more frequently observed at night than during daytime (e.g. Brinkmann, 1974; Jiang and Doyle, 2008; Valkonen *et al.*, 2010).

Mountain flows have been diagnosed through a number of different parameters. A central parameter in this respect is the non-dimensional mountain height Nh/U (also known as the inverse Froude number) (e.g. Smith and Grønås, 1993), in which N is the Brunt–Väisälä frequency, h is the obstacle (mountain) height, and U the typical wind speed of the upstream background flow. Based on this parameter, Smith (1989) describes the following basic flow regimes. Low values of Nh/U enable the flow to pass over the mountain without any upstream stagnation and typically gentle gravity waves are formed. Nh/U can be seen as a measure of the nonlinearity in the flow, and linear theory

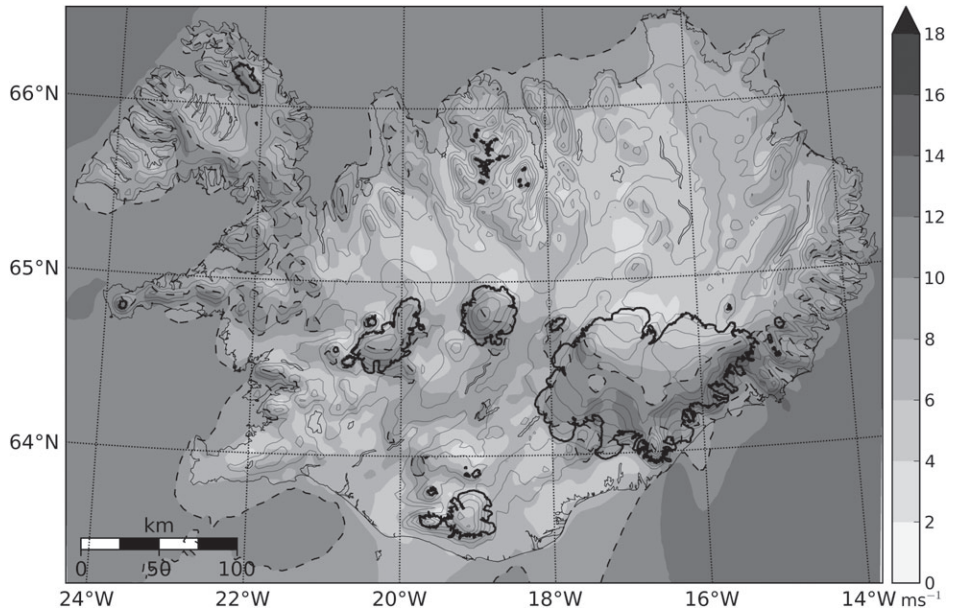

Figure 1. Mean near-surface wind speed over Iceland for cases with northeasterly flow (shading, 2 m s^{-1} intervals). The 10 m s^{-1} limit is indicated by a dashed grey line. The results are based on ECMWF analysis data downscaled with WRF at a 3 km horizontal resolution for the years 1995–2008. Terrain countours are given every 200 m and the major ice caps are outlined. The location of the area in Figure 2 is indicated by a black rectangle.

describes the flow response for values of Nh/U well below unity (Gill, 1982). For values of Nh/U close to unity, the flow enters a high drag state. In this state, there are typically amplified and even breaking gravity waves and strong downslope flow acceleration on the mountain's lee side. For increasing values of Nh/U, the waves gradually become less prominent, while an upstream blocking is a more dominant feature in the flow morphology.

In the present study, flow over the Hofsjökull ice cap in Central Iceland is explored. The flow is simulated with realistic surface conditions and compared to observations that were made during the Flow over and around Hofsjökull (FLOHOF) field campaign in 2007 (Reuder *et al.*, 2012). In a set of numerical sensitivity experiments, the flow is also simulated with increased surface friction and no ice cover in the area presently covered by ice. The purpose of the study is primarily to explore the response of the flow field over Hofsjökull to modified surface characteristics corresponding to the melting of the Hofsjökull's ice cap. Ice caps are both smooth and cold and we seek to find out which of these properties is more important for enhancing the downslope winds over Hofsjökull in our case study.

The study is motivated by indications of prominent downslope windstorms over Hofsjökull (Rögnvaldsson *et al.*, 2007). The study is also motivated by the predictions of climate change leading to the disappearance of ice caps. Ice caps are generally much smoother than their underlying surface and they prevent the surface temperature from rising above 0 °C. The latter may locally increase the ABL's static stability, particularly during daytime in the summer.

The reduction or enhancement of mountain waves through the above-described processes have potentially large impacts on the general atmospheric circulation. Orographic drag connected to mountain gravity waves is a significant sink in the atmospheric momentum budget (e.g. Lilly, 1972; Wahr and Oort, 1984). Aloft, amplified and breaking gravity waves are known to be potentially hazardous for aviation (e.g. Ólafsson and Ágústsson, 2009; Lane *et al.*, 2009). Close to the ground, corresponding downslope accelerated flow may be a risk for human activities and constructions (e.g. Stewart *et al.*, 2005).

2. Climatology of summertime northeasterly flow over Iceland and Hofsjökull

We will first consider a dataset from the 'Reikningar á veðri' (RÁV) project (Rögnvaldsson *et al.*, 2007) to briefly investigate the climatological mean wind patterns over Iceland in general and Hofsjökull in particular. The investigation is focused on northeasterly flow. As described in Rögnvaldsson *et al.* (2007), the RÁV dataset is constructed by dynamically downscaling the analyses from the European Centre for Medium-range Weather Forecasting (ECMWF) using the Weather Research and Forecasting (WRF) model (Skamarock *et al.*, 2008), with a horizontal resolution of 3 km for the years 1995–2008. The ECMWF ERA-40 reanalysis is used for the years 1995–2000 and the ECMWF operational analysis is used after the year 2000. The set-up of the WRF model was similar to that employed for the numerical simulations of this study, described in section 4.1.

Figure 1 shows the mean near-surface wind speed over Iceland in the RÁV dataset for situations with wind speeds above 5 m s^{-1} and wind directions within the sector $45 \pm 22.5^{\circ}$ over the top of Hofsjökull for the months June, July, August, and September. This wind sector constitutes 17% of all winds during this time of the year. At the coast during northeasterly summertime flow, the lowest wind speeds are found in the northeast and in the southwest of Iceland. The geographical locations and spatial extents of these minima suggest that they are associated with large-scale blocking and wake effects. Offshore, the strongest winds are found along the southeastern and northwestern coast, as may be expected for a flow accelerating past a barrier. Onshore, the strongest winds are found above the downstream slopes of the larger ice caps. A closer look at the region of interest near the Hofsjökull ice cap (Figure 2) reveals relatively low wind speeds immediately upstream and a few kilometres downstream of Hofsjökull, indicating local blocking and wake effects. The strongest wind speed is located downstream of the mountain top, and there is a layer of significantly weaker winds aloft above the lee-side slope, indicative of downslope acceleration associated with gravity wave activity (Figure 3).

3. Observations from the FLOHOF field campaign

3.1. *The FLOHOF field campaign*

The observational data used in the present study were obtained during the Flow over and around Hofsjökull (FLOHOF) field campaign. The campaign took place from 21 July to 24 August 2007, in the area of the Hofsjökull mountain ice cap in Central Iceland. The campaign was targeted towards investigating the response of mountain waves to changes in upstream flow conditions with time. Hofsjökull (1782 m above sea level, asl)

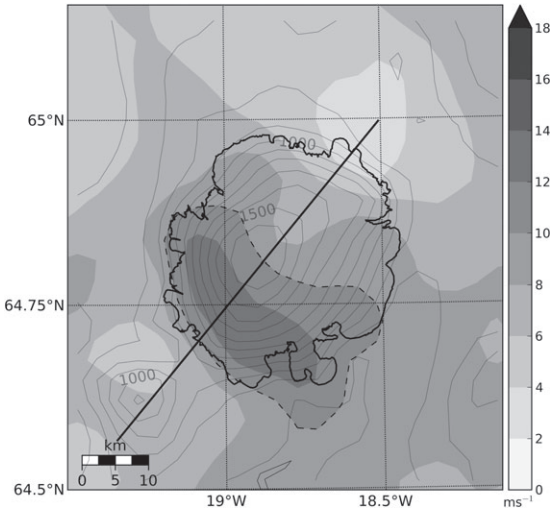

Figure 2. As Figure 1, but for an area around Hofsjökull in Central Iceland. The location of the vertical cross-section in Figure 3 is indicated by the diagonal black solid line.

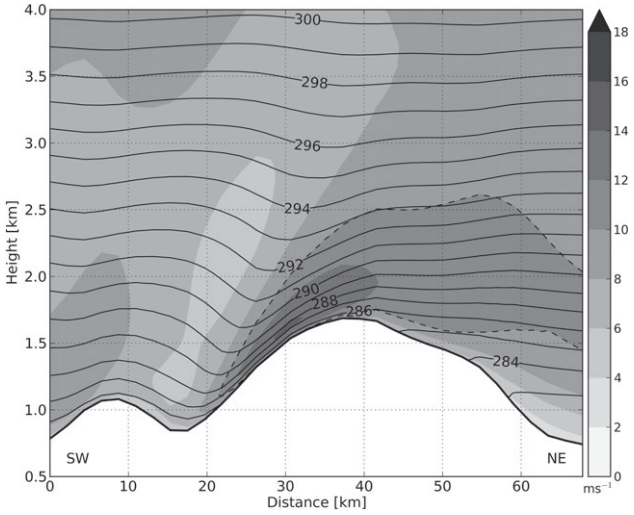

Figure 3. Vertical cross-section of mean horizontal wind speed (shading, 2 m s^{-1} intervals) and potential temperature (K) over Hofsjökull. The 10 m s^{-1} limit is indicated by a dashed grey line. The results are based on ECMWF analysis data downscaled with WRF at a 3 km horizontal resolution for the years 1995–2008. The location of the cross-section is indicated in Figure 2. The mean flow direction is from the right (northeast) to the left (southwest).

rises some 1000 m above its surroundings and has a diameter of 30–40 km. Its unique, nearly circular shape and smooth, ice-covered surface makes it ideal for the study of mountain flows. The limit of permanent snow/ice follows roughly the 1000 m contour. A more detailed description of FLOHOF can be found in Reuder *et al.* (2012).

3.2. *Automatic weather stations*

During the FLOHOF campaign, there was a network of 19 automatic weather stations (AWSs) on and around Hofsjökull. The stations measured temperature, wind direction, wind speed, relative humidity, pressure and, precipitation. When positioning the AWSs, emphasis was put on obtaining a homogenous network of measurements. However, the eastern and western parts of the ice cap proved hard to reach and no stations could be erected there. The AWSs were inspected regularly during the campaign to ensure continuous data series, but icing of the wind sensors did occur in some cases, especially of those situated on the ice cap during northerly flow. Data from stations experiencing icing are not included in the present study.

3.3. *Small unmanned meteorological observer (SUMO)*

The atmospheric profiles used for model validation in the present study were obtained from a location southwest of Hofsjökull (Figure 4) using the Remotely Piloted Aircraft System (RPAS) SUMO. The SUMO aircraft features an advanced on-board navigation system and it can be programmed to perform various flight patterns. When operated for atmospheric soundings, as done in this study, the SUMO flight pattern resembles a helix corresponding to an atmospheric column with a radius of 50–100 m. More detailed information on SUMO can be found in Reuder *et al.* (2009) and Mayer *et al.* (2012b).

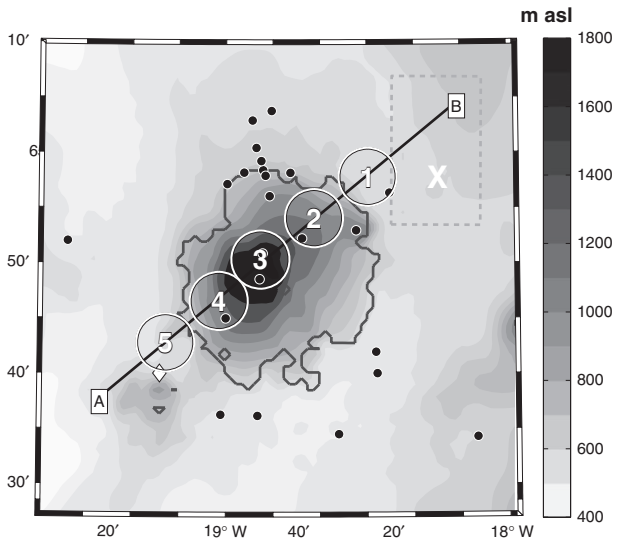

Figure 4. Map of the Hofsjökull area (corresponding to domain 3). Terrain height is indicated with grey shading (200 m intervals). The white circles, numbered from 1 to 5, indicate the locations of the areas upstream, upslope, mountain top, downslope and downstream. The solid, black line A–B marks the location of the time-averaged wind profiles in Figure 10 and vertical cross-sections in Figures 15 and 16. The white diamond is the RPAS SUMO launch location. The black dots mark the locations of the AWSs in the area. The Hofsjökull ice cap is encircled by a dark grey solid line. Temperature and wind profiles from a vertical column spanning the grey dashed rectangle in the upper-right corner (marked by 'X') are used to estimate upstream flow conditions.

4. Numerical simulations

4.1. *High-resolution simulations*

The atmospheric flow above Mount Hofsjökull on 13 and 14 August 2007 is simulated at high horizontal resolution using the WRF model. The model is initialised and forced at its boundaries with model-level data (91 vertical levels) from the ECMWF operational analysis with a horizontal resolution of 0.25°. It is run at a resolution of 9, 3 and 1 km with respectively 85×90, 187×157 and 82×82 gridpoints in the two-way nested domains (Figure 5). There are 51 model levels in the vertical, which are terrain-following at lower levels but flatten gradually towards the top of the model at 50 hPa. The lowest first few model half-levels are situated at about 9, 33, 72, 114, 156 and 200 m above ground level (agl). Similar horizontal and vertical grid resolutions have previously been used in studies by e.g. Kilpeläinen *et al.* (2011), Mayer *et al.* (2012c) and Ágústsson and Ólafsson (2012).

The model is run for a total of 30 h, starting at 0000 UTC on 13 August 2007 and the first 6 h are considered spin-up and therefore not included in the analysis part of this study. We will quote the times of day as UTC, which is equal to the local Icelandic time. The local noon is shortly after 1300 UTC. The Mellor–Yamada–Janjić scheme (Mellor and Yamada, 1982; Janjić, 1994, 2001) is used for boundary-layer parametrization. This scheme is a 1.5-order local scheme, where the turbulent kinetic energy (TKE) is calculated through a prognostic equation and the diffusion coefficient is

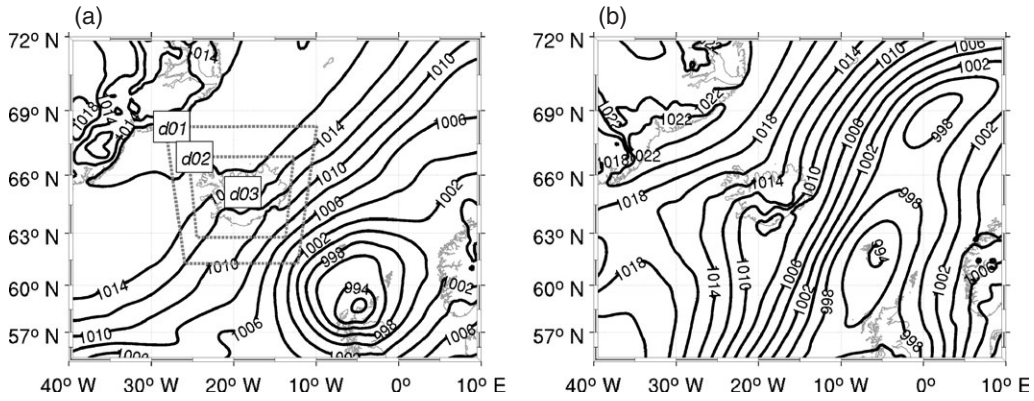

Figure 5. Mean sea level pressure (hPa) at (a) 1200 UTC on 13 August 2007 and (b) 1200 UTC on 14 August 2007 obtained from the ECMWF operational analysis. The locations of the three WRF domains for the numerical sensitivity experiments are shown in (a).

Table 1. Numerical sensitivity experiments, corresponding model surface types and surface type parameters as used in WRF. The surface type refers to the model land use covering the extent of the Hofsjökull ice cap, as shown in Figure 4.

Experiment	Surface type	z_0 (m)	Albedo (%)	Emissivity (%)	Soil moisture (%)
Smooth glacier (ctrl)	Snow or ice	1×10^{-3}	55	92	95
Rough noglacier	Mixed tundra	1.5×10^{-1}	15	95	50
Rough glacier	Snow or ice	1.5×10^{-1}	55	92	95
Smooth noglacier	Mixed tundra	1×10^{-3}	15	95	50

computed as a function of the Richardson number and the TKE. The RRTM scheme (Mlawer *et al.*, 1997) is employed for long-wave radiation, the Dudhia scheme (Dudhia, 1989) for short-wave radiation, and the Unified NCEP/NCAR/AFWA* Noah land-surface model (Chen and Dudhia, 2001) with soil temperature and moisture in four layers for surface physics. The parametrization of microphysics is done using the WRF single-moment (WSM) three-class simple ice scheme (Dudhia, 1989; Hong *et al.*, 2004), which includes cloud water/ice and rain/snow as prognostic variables. Apart from the innermost domain, the set-up is nearly identical to that of the numerical simulations by the Institute for Meteorological Research (IMR; http://www.riv.is; accessed 15 December 2013) which are used for operational forecasting at the Icelandic Meteorological Office (Veðurstofa Íslands) and published online at http://belgingur.is (accessed 15 December 2013). Since the Icelandic ice caps in the default WRF land-use dataset from the US Geological Survey (USGS) are too large, we use an updated version of the USGS land-use dataset with more realistic ice-cap extents provided by IMR.

4.2. *Sensitivity experiments*

Four numerical simulations have been made in this study, each with different combinations of model land use and roughness length of momentum (z_0) over the Hofsjökull ice cap. The first simulation is the control simulation, here referred to as 'smooth glacier (ctrl)' for consistency with the names of the other simulations. In the 'smooth glacier' simulation, the original USGS 'snow or ice' land use is kept and the z_0 over the ice cap is 1×10^{-3} m. In the second simulation, 'rough noglacier', the 'snow or ice' land use on the ice cap of Hofsjökull is replaced with the land surface dominating the ice cap's surroundings, called 'mixed tundra', which has a z_0 of 1.5×10^{-1} m. In the third simulation, 'rough glacier', the land use is kept as default, i.e. with an intact ice cap, but with a z_0 for the 'snow or ice' land-use category set to 1.5×10^{-1} m. In the fourth simulation, 'smooth noglacier', the land use over Hofsjökull is set to a dummy land-use category that shares all properties (e.g. albedo, emissivity and moisture availability) with 'mixed tundra' except z_0, which is equal to that of 'snow or ice'. An overview of the simulations and their respective land-surface properties is given in Table 1.

In reality, the z_0 over glaciers may vary considerably in both space and time. Smeets and van den Broeke (2008) investigated the z_0 over the melting (ablation) zone of the Greenland ice sheet. They found values of z_0 of the order of 1×10^{-5} m for an area close to the glacier's equilibrium line, whereas they estimated a z_0 larger than 1×10^{-2} m for lower parts of the ablation area in the summer where snow melting uncovers ice hummocks. The Hofsjökull ice cap's default z_0 of 1×10^{-3} m in our study is close to the average of the values estimated by Smeets and van den Broeke (2008). For comparison, the review by Stull (1988) gives a z_0 of ice of the order of 1×10^{-5} m and a z_0 of snow of the order of 1×10^{-4} m.

During the winter, the entire area around Hofsjökull is covered with snow most of the time and the changes in model surface land use ('snow or ice' versus 'mixed tundra') are therefore not meaningful for the flow at this time of the year.

5. Results

5.1. *Case-study, 13 and 14 August 2007*

During 13 and 14 August 2007, Iceland was embedded in northeasterly flow set up by low pressure over the British Isles and high pressure over Greenland (Figure 5). A detailed overview of the near-surface flow over Iceland on 13 August is given in Figure 6. The figure displays the simulated near-surface (9 m agl) wind speed and direction at 1200 UTC in domain 2 (3 km horizontal resolution). The wind field bears a close resemblance to the average winds for northeasterly flow situations as calculated from the climate simulations for Iceland (Figure 1). Offshore, the strongest winds are found in the southeast and the weakest winds are found in the wake to the south of Iceland. Over land, the strongest winds are located above the downstream slopes of the large ice caps. In domain 3 (Figure 7, 1 km horizontal resolution), located over the area of Hofsjökull, the downstream acceleration of winds over the ice cap is more clearly seen. The simulated flow compares reasonably well to available AWS data spread around Iceland for domain 2 and the AWS on and around Hofsjökull for domain 3. The wind speed measured by the AWS on the lee-side slope of Hofsjökull confirms the relatively strong downslope

*(US) National Centers for Environmental Prediction/National Center for Atmospheric Research/Air Force Weather Agency

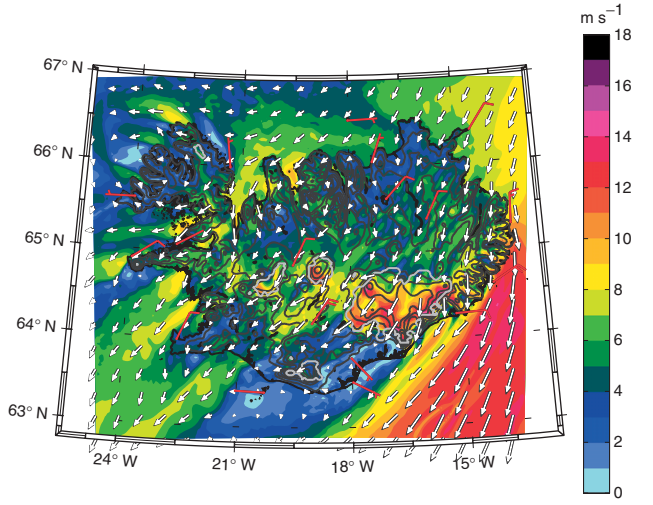

Figure 6. Simulated near-surface wind speed (shading, 1 m s^{-1} intervals) from the ctrl simulation at 1200 UTC on 13 August for domain 2 (3 km horizontal resolution). Surface observations from AWSs are indicated by wind barbs; each half barb is 2.5 m s^{-1}. Terrain contours are given every 250 m and the major ice caps are outlined.

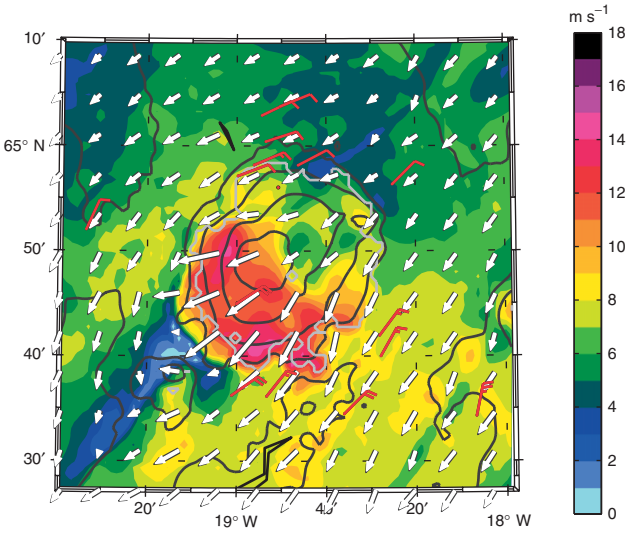

Figure 7. As Figure 6, but for domain 3 (1 km horizontal resolution).

wind. A more detailed model validation against the AWS data can be found in Mayer *et al.* (2012a), who used the same basic model set-up as in the present study to simulate cases from FLOHOF.

During 13 August, several soundings were made with the RPAS SUMO downstream of Hofsjökull. These soundings (Figures 8 and 9) reveal a multi-layered atmospheric structure from the ground level up to around 1200 m agl, which is slightly higher than the height of Hofsjökull above its surroundings. The wind direction below 1200 m agl varies between northeasterly and southeasterly in the first two profiles (1325 and 1407 UTC) and the wind speed is below 5 m s^{-1} down to about 100 m agl where it increases again somewhat. The wind direction is more easterly (approximately 45°) in the last profile (1742 UTC) below 1200 m agl than in the two earlier ones, coinciding more closely with what can be considered as the synoptic wind direction farther aloft. This lower layer (below 1200 m agl) is capped by a wind minimum in all three profiles. Correspondingly, there is a weak inversion and a drop in humidity at the top of this layer. At higher elevations, 1800–2000 m agl, there is a stronger temperature inversion than that found closer to the ground level. This inversion is situated slightly below a wind maximum exceeding 10 m s^{-1}. A similar inversion is observed in the Keflavík sounding in southwest Iceland (not shown), which might indicate the presence of a larger-scale subsidence inversion.

In spite of the large spatial and temporal flow variability, the model reproduces the observed temperature, humidity, and wind patterns quite well. The simulated spatial variability in wind is particularly large below 1200 m agl, as indicated by the grey bars around the simulated profiles, showing the minimum and maximum values within an atmospheric column of size 4 × 4 km.

5.2. *The simulated flow over and around Hofsjökull and its sensitivity to surface characteristics*

Figure 10 shows the wind speed across Hofsjökull averaged over the three lowest model levels (9, 35 and 70 m) for the whole simulation period (24 h). Over the mountain surface, the wind speed in the simulations with a smooth surface is consistently higher than in the simulations with a rough surface. Upstream of the ice cap, where the surface land-use characteristics are the same in all simulations, the difference in wind speed between the simulations is minimal. The sensitivity to the surface roughness is by far largest over the lee-slope of the mountain, where the wind speed is much lower in the rough surface simulations than in the smooth surface simulations. The smoother surfaces lead to a slightly longer average downstream extent of the strong downslope flow than their rougher counterparts. The sensitivity in the wind speed to the surface's thermal properties ('glacier' versus 'noglacier') is lower than that to the surface roughness, but also this sensitivity is mainly visible over the lee slope. There, the mean wind speed is about 1 m s^{-1} higher in the 'glacier' simulations than in the 'noglacier' simulations along the investigated cross-section.

5.3. *The flow aloft in the lee of Hofsjökull*

Figure 10 gives a picture of the net effects of the surface characteristics on the flow over Hofsjökull for the whole simulation period for the selected cross-section. However, it does not tell us how the effects and the flow itself vary with time and in space. We start by investigating the time-dependent variability and for this investigation we consider the near-surface wind speed in five areas situated across the mountain, each of which are associated with characteristic locations and flow patterns. We refer to the areas as upstream, upslope, mountain top, downslope, and downstream (Figure 4). The wind speed in each area is shown in Figure 11(a)–(e). Secondly, we know from previous literature (Introduction and references therein) that surface temperature and surface heat fluxes potentially affect downslope flow. In a real flow study like the present one, these parameters will naturally vary with time and changing land-use type from 'snow or ice' to 'mixed tundra' will modify them further. Time series of temperature and heat flux averaged over the surface of Hofsjökull are presented in Figure 11(f)–(g). Lastly, profiles of temperature, wind speed and wind direction from a location upstream of Hofsjökull are shown in Figure 12.

In the upstream area, which is located off the ice cap, the wind speed is virtually unaffected by the modified mountain surface characteristics throughout the simulation period. In that area, the highest wind speed is found during daytime and the lowest during night-time in all four simulations. This suggests that mixing of the ABL is most important for the temporal variability of wind speed in this area. Indeed, the upstream temperature profiles reveal a well-mixed boundary layer reaching up to about 500 m agl in the daytime. Above, the air mass is stably stratified. In the night (0000 UTC) and early morning (0600 UTC), the entire air mass is stably stratified. The wind speed in the lower part of the upstream profiles also follows a diurnal pattern with the highest wind speeds during daytime and the lowest during night-time. The wind direction remains within 35–60°. Elevated inversions are known to affect mountain flow (Introduction), but no such inversion is present at any time of the day in our simulations. A diurnal signal in the wind speed is also evident in the downstream area.

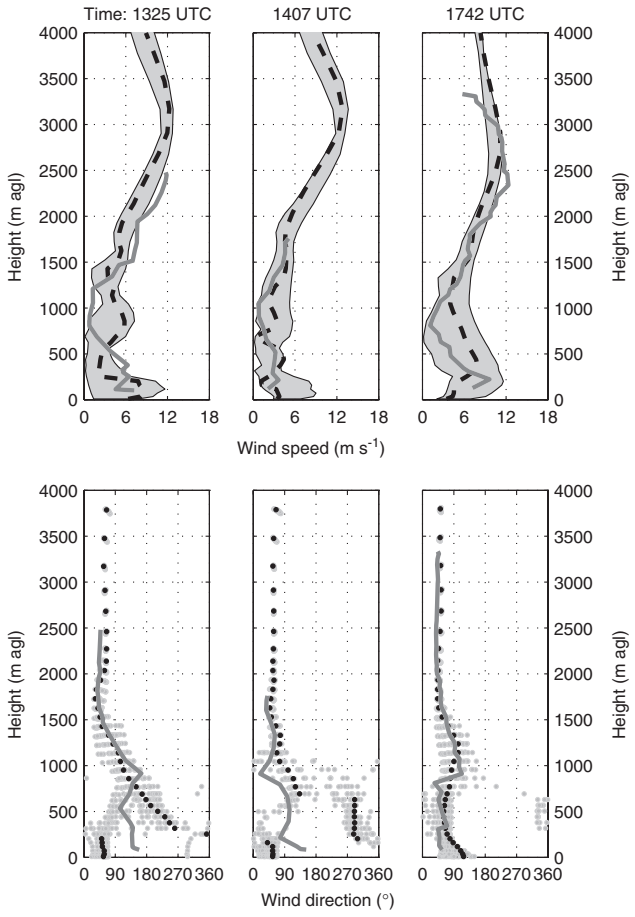

Figure 8. Observed and simulated vertical profiles of wind speed ($m\,s^{-1}$) and wind direction (°) on 13 August 2007 downstream of Hofsjökull (location indicated in Figure 4). Dark grey, solid lines are the observations and dashed, black lines (black dots for the wind direction) are the simulated profiles from the grid point closest to the observation location. The grey bands (grey dots for the wind direction) represent the spread in simulated wind speed and wind direction within an atmospheric column that spans 4×4 km in the horizontal and which is centred at the closest grid point.

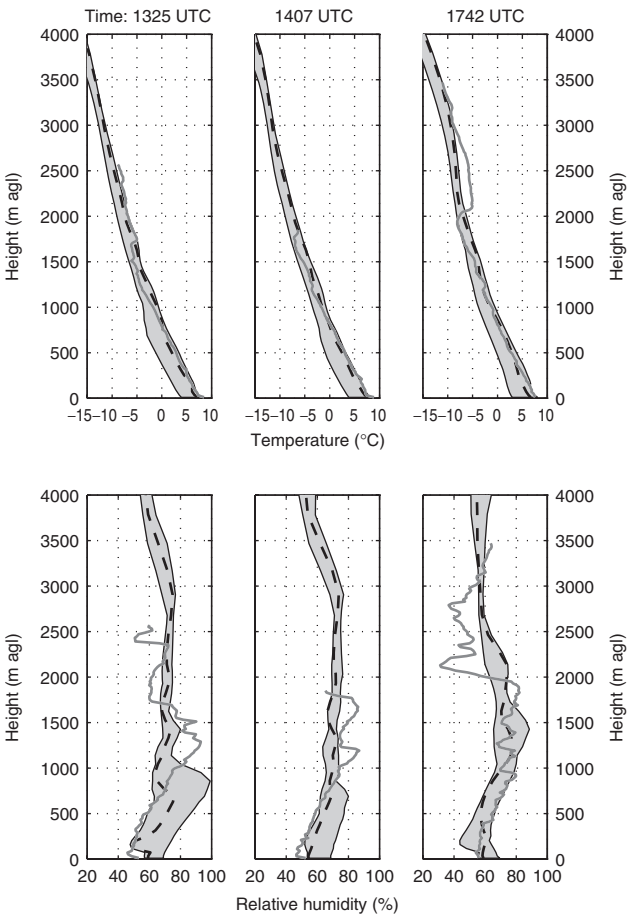

Figure 9. As Figure 8, but for temperature (°C) and relative humidity (%).

The control simulation ('smooth glacier') captures reasonably well the observed low-level flow downstream of Hofsjökull, measured between 1200 and 1800 UTC on August 13 (Figure 8), with relatively high wind speeds (around $8\,m\,s^{-1}$) in an approximately 100 m deep layer near the ground. Interestingly, at the same time, there is a large difference in wind speed between the 'smooth' and 'rough' simulations in the downstream area. The extent of the downslope accelerated flow is greatest in the simulations with the smooth mountain surface, and the flow extends well into the downstream area. In the 'rough' simulations, the flow stops short of the downstream area. Possible dynamical reasons for the temporal variability in the flow regime over Hofsjökull are discussed later in this section and related to upstream flow parameters.

In the areas located over the mountain surface, i.e. upslope, mountain top and downslope, an increased surface roughness mostly leads to lower wind speeds. An exception is the period from 0000 to 0600 UTC on 14 August in the upslope area, where the effect is minimal. As for the cross-sections in Figure 10, the damping of the wind by increased surface roughness is largest over the downslope area (Figure 11(d)). Also the effect of increasing the surface temperature is largest over that area, while the signal of surface heating is not consistent in time over the downstream area (Figure 11(d)). Over the downslope area, the wind speed over the colder surface ('glacier' simulations) is consistently higher than over the warmer surface ('noglacier' simulations). Since the surface temperature cannot exceed 0 °C in the 'glacier' simulations, its amplitude is naturally smaller than in the 'noglacier' simulations, where it peaks at around 6 °C (Figure 11(f)). The surface heat flux over the mountain (Figure 11(g)) follows the same temporal pattern as the mountain surface skin temperature. The skin temperature upstream of the mountain follows roughly the oscillation of the 'rough noglacier' simulation in Figure 11(f), and this is reflected in the profiles of wind and temperature in Figure 12.

Before moving on to an analysis of the spatial variability in the flow field over Hofsjökull and its sensitivity to the surface characteristics, we consider in more detail the temporal variability in the upstream flow characteristics. Central parameters in this respect are the upstream flow speed, U, and the Brunt–Väisälä frequency, N, the latter being defined as

$$N = \sqrt{\frac{g}{\theta_{\mathrm{avg}}} \frac{\mathrm{d}\theta}{\mathrm{d}z}}, \tag{1}$$

where g, θ and z are the acceleration of gravity, the potential temperature and the altitude. θ_{avg} is the average potential temperature within the atmospheric layer for which N is calculated. Estimating U and N for real atmospheric flow can be a challenging task and several solutions have been proposed. In this study, we use the vertical averaging operator

$$B = \frac{\sum_{i=1}^{n-1} A_i (z^*_{i+1} - z^*_i)}{\sum_{i=1}^{n-1} (z^*_{i+1} - z^*_i)} \tag{2}$$

to calculate U and N. In Eq. (2), the parameter over which we average is denoted A and the resulting averaged parameter is denoted B. The averaging is done for U and N separately from the surface (n = 1) and up to the 28th model level (n = 28), which is situated at around 2000 m agl. The calculation is weighted by

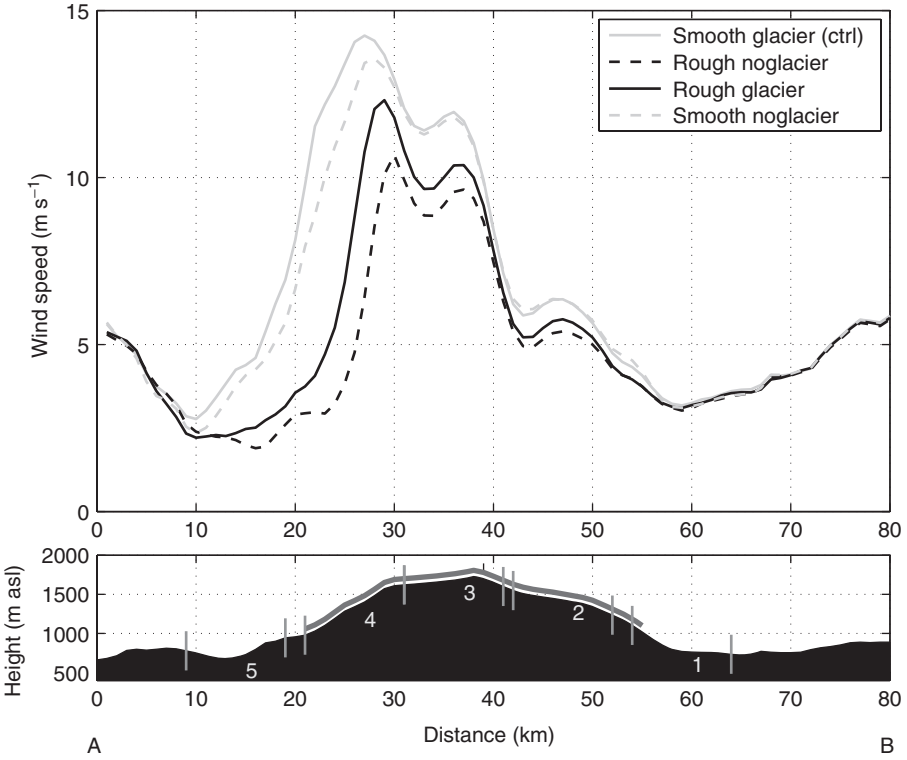

Figure 10. Cross-section of mean simulated near-surface wind speed ($m\,s^{-1}$) (average of the three lowest model levels) over the simulation period for the four different sensitivity experiments. The mean flow direction is from the right (northeast) to the left (southwest). The location of the cross-section and the areas marked with numbers from 1 to 5 referred to as upstream, upslope, mountain top, downslope and downstream, are indicated in the lower panel and in Figure 4. The location of the ice cap is indicated with a solid grey line above the mountain topography in the lower panel.

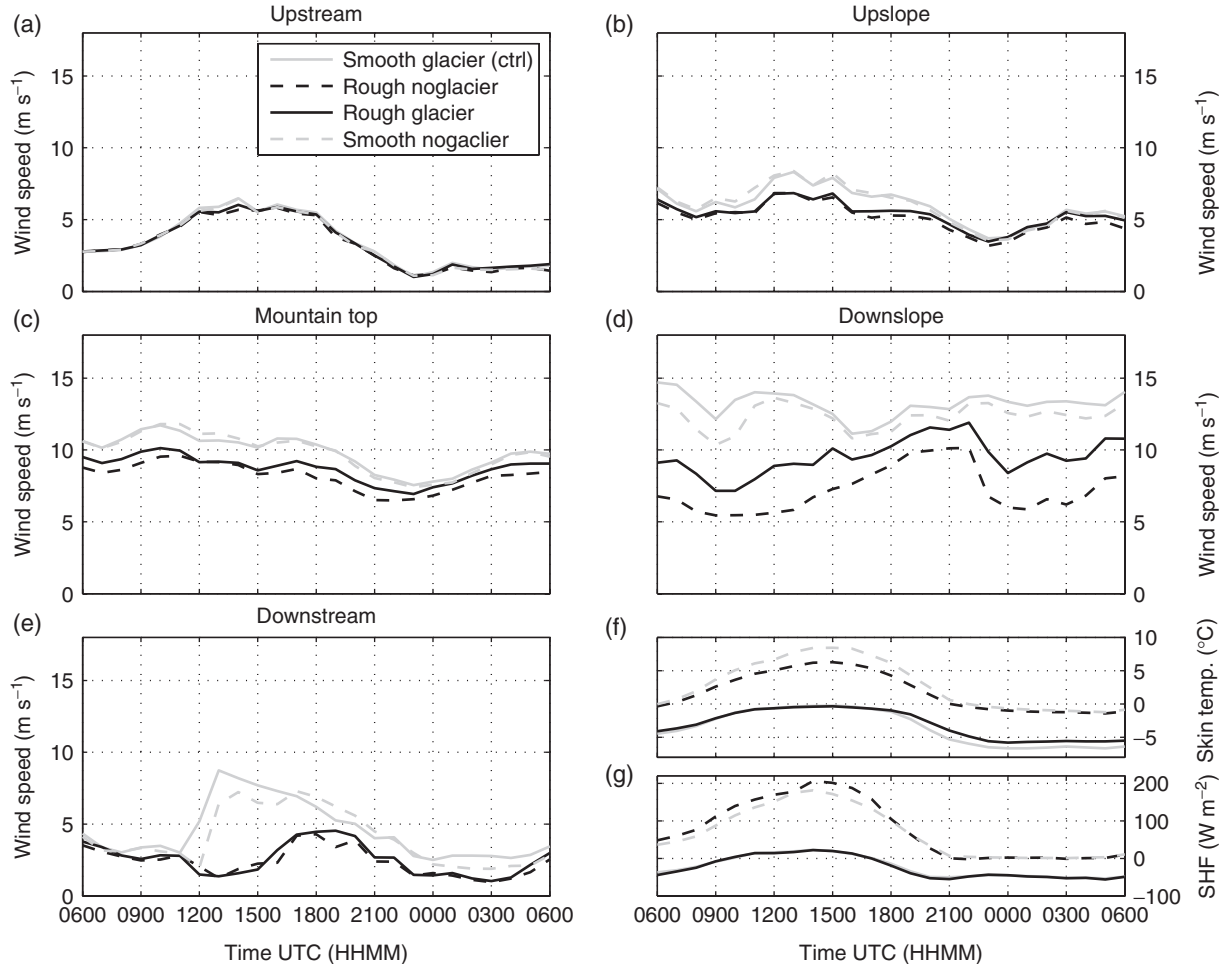

Figure 11. Simulated near-surface wind speed ($m\,s^{-1}$) (average of the three lowest model levels) on 13 and 14 August 2007 for five areas on and near Hofsjökull associated with five characteristic locations and flow patterns: (a) upstream, (b) upslope, (c) mountain top, (d) downslope and (e) downstream for the four different simulations. The location of the five areas are indicated in Figure 4. (f) and (g) show respectively the average skin temperature (°C) and the average sum of the surface sensible and latent heat fluxes (SHF, $W\,m^{-2}$) over the ice cap of Hofsjökull.

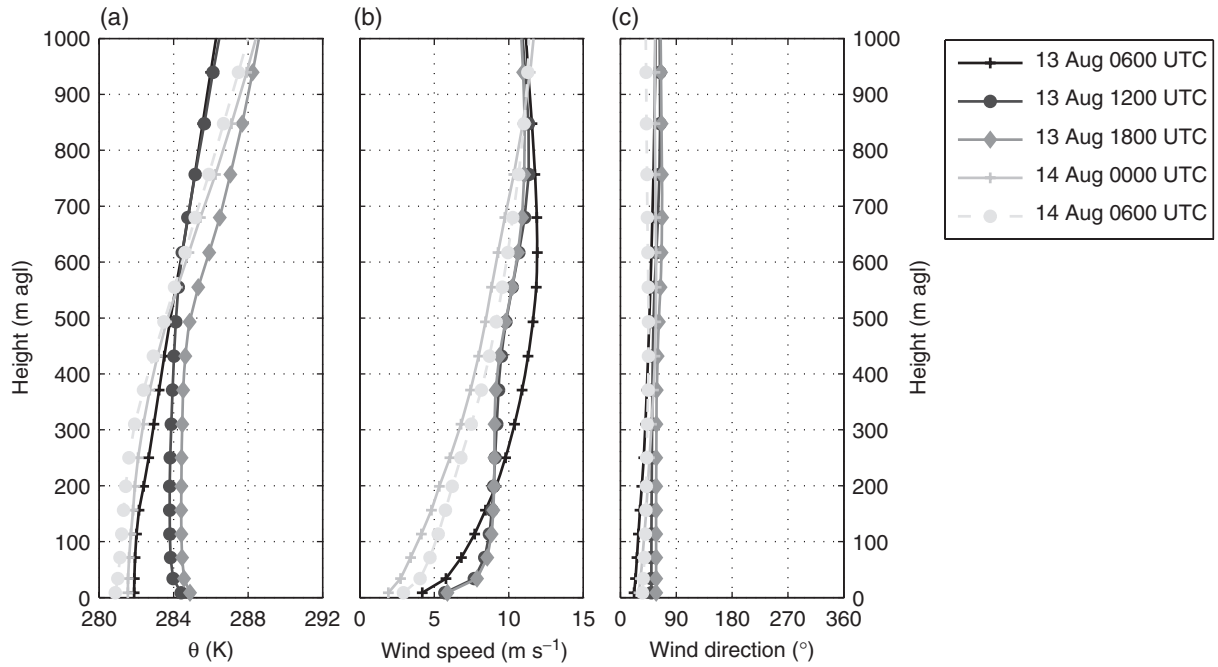

Figure 12. Profiles of (a) potential temperature (θ; K), (b) wind speed (m s^{-1}) and (c) wind direction (°). The profiles are all from the ctrl simulation and are obtained from horizontal grid averages within the column marked 'X' in Figure 4.

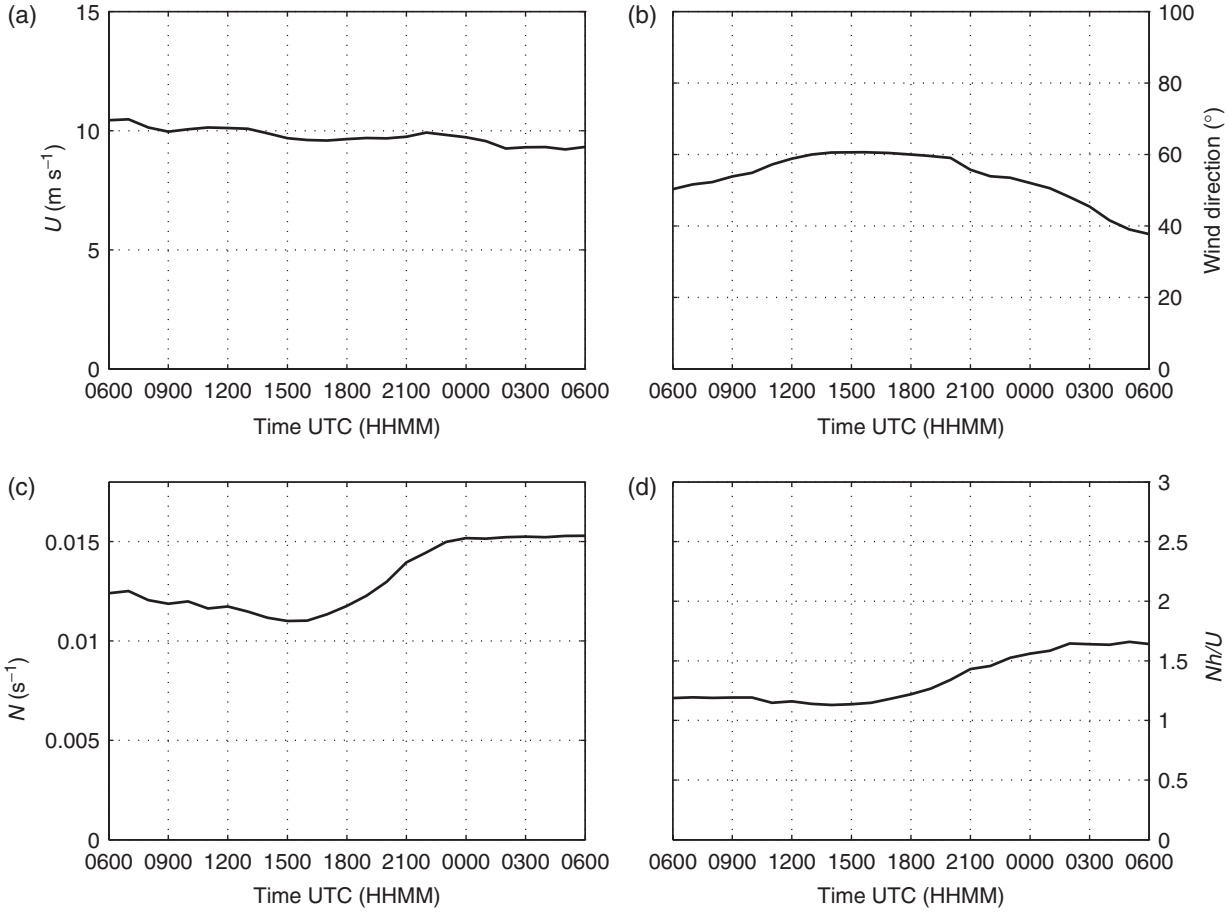

Figure 13. Simulated upstream flow parameters from the ctrl simulation (a) U (m s^{-1}), (b) wind direction (°), (c) N (s^{-1}) and (d) Nh/U. U and N have been calculated separately and averaged horizontally over all model levels between the surface and 2000 m agl within an atmospheric column located upstream of the Hofsjökull ice cap (marked 'X' in Figure 4).

the depth of each layer, i.e. $(z^*_{i+1} - z^*_i)$, where z^* is the elevation of each model level. h is set to 1000 m, which is the height of Hofsjökull above its surroundings. The layer between the surface and $2h$ (around 2000 m) is the air mass that is most affected by the presence of the mountain, and the mountain crest is in the middle of this layer. A similar procedure for calculating U and N was used by Ólafsson and Bougeault (1997a). Examples of other studies where U and N have been calculated using separate averaging of the variables include Chen and Smith (1987) and Georgelin *et al.* (1994).

From Figure 13, we see that the stability N and the boundary-layer height (as deduced from Figure 12(a)) both feature a typical diurnal variability. The highest values of N are found during night-time and the lowest values during daytime. The values of

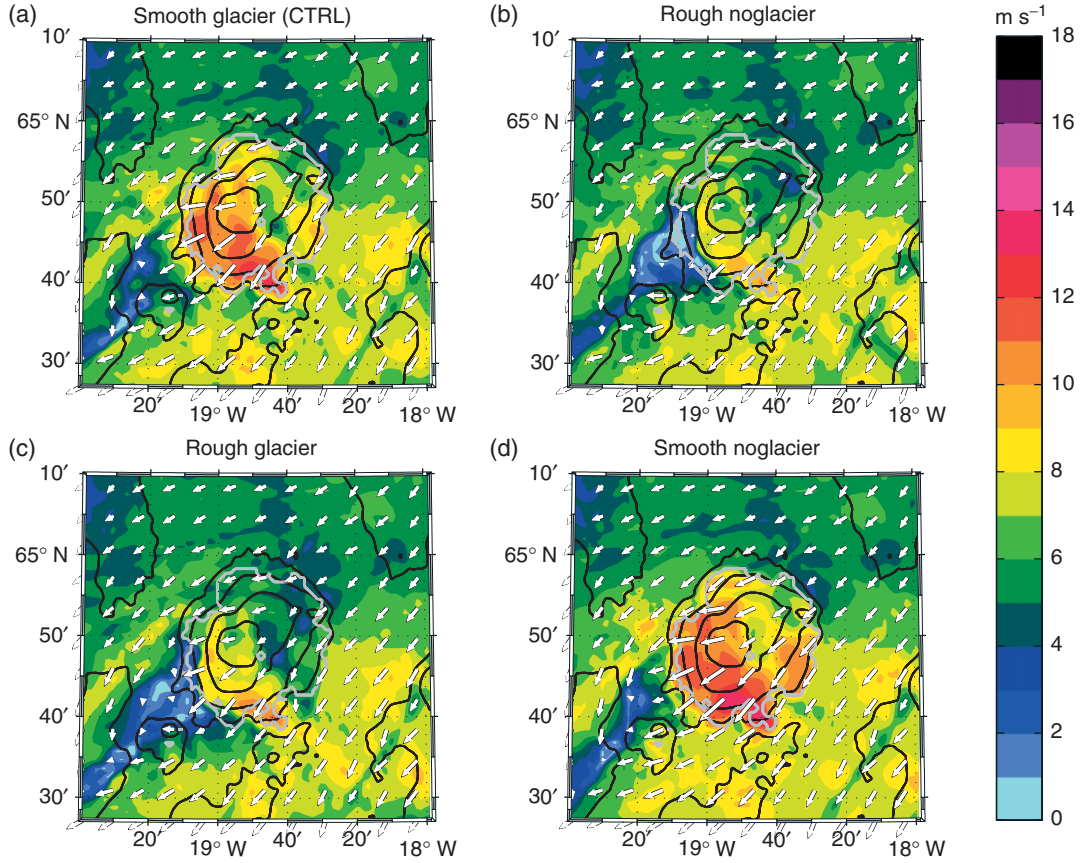

Figure 14. Simulated near-surface wind speed (lowest model half-level, ∼ 9 m agl (shading, 1 m s^{-1} intervals) over Hofsjökull at 1500 UTC on 13 August 2007 from the simulations: (a) smooth glacier (ctrl), (b) rough noglacier, (c) rough glacier, and (d) smooth noglacier. The grey solid line around Hofsjökull indicates the location of the ice cap. The terrain height is given by contours every 250 m.

Nh/U, which vary between 1.1 and 1.6, follow the same temporal pattern as N. The value of the non-dimensional number governing non-hydrostatic effects, Na/U, is between 38 and 66, where a is the streamwise mountain width set to 40 km. This means that the flow is fairly hydrostatic. The average upstream wind speed U varies between 8.5 and 10.5 m s^{-1}, and the average upstream wind direction stays between 35 and 60°, implying a moderate northeasterly flow throughout the simulation period.

In the horizontal wind field over Hofsjökull at 1500 UTC (Figure 14), we can clearly see how the downslope wind speed and its horizontal extent are greater in the smooth surface simulations than in the simulations with a rough surface. The differences amount to about 5 m s^{-1} and 5–10 km, respectively. On the other hand, the differences in the downslope flow between the simulations with and without the ice cap are only marginal and furthermore they are inconsistent in space. For some areas, the flow is stronger in the simulations with the ice cap, while for other areas the opposite is the case. Thus, based on our four simulation experiments, we cannot draw any consistent conclusions regarding the sensitivity of the flow to changes in the surface temperature. An investigation of horizontal flow fields for the rest of the simulation period (not shown) also remains inconclusive in this regard.

Aloft, in the vertical cross-sections (Figure 15), there are close to vertical and even backwards tilting/overturning isentropes above the mountain's lee-side slope. This flow pattern indicates the presence of breaking internal gravity waves (IGWs) and these waves can be assumed to be the cause of the downslope accelerated flow. The wave pattern/amplitude is very similar in all four simulations and the waves themselves thus appear to be relatively insensitive to the changes in surface characteristics. The described flow pattern is coherent with what one would expect for Nh/U around 1.1 that we find for this time of the day (Smith, 1989). The downslope flow in the smooth surface simulations (Figure 15(a, d)) reaches 5–10 km farther downstream than in the rough surface simulations (Figure 15(b, c)). There is also a slight difference between the 'noglacier' and 'glacier' experiments, the latter tending to have a marginally longer downslope accelerated flow. However, as seen in the horizontal wind fields (Figure 14), this sensitivity is not consistent in space.

At 0300 UTC on 14 August (Figure 16), Nh/U has increased to around 1.6, resulting from a slight decrease in U and an increase in N (Figure 13). Increasing Nh/U beyond 1 typically leads to a damped wave activity and an increased tendency for upstream blocking along with a less pronounced downslope accelerated flow (Smith, 1989). This is precisely what we see when we compare the flow at 0300 UTC to the flow at 1500 UTC the day before. The downslope flow extends for a shorter distance downstream, there is slightly lower wave activity and the waves are somewhat less steep (less breaking) in the night than during the day. Furthermore, there are signs of upstream blocking during the night. This night-time upstream flow deceleration can be recognised in both the upstream wind profiles in Figure 12(b) and in the wind speed in the upstream area in Figure 11(a).

Regarding the downslope accelerated flow's sensitivity to the surface characteristics, the same conclusions can be drawn for the night as for the day; the effect of an increased surface friction on the downslope flow acceleration is significant, while the impact of modified surface temperatures is marginal along the investigated cross-section. As during the day, the impact of the modified surface characteristics over Hofsjökull on the IGW remains insignificant at night.

In summary, the changes in surface characteristics over Hofsjökull's ice cap locally perturb the downslope flow in terms of altering its speed and downstream penetration. In this regard, the impact of the modified surface roughness is, in contrast to the impact from modified surface temperatures, large and consistent in both space and time. The overall flow features, like lee-side wave amplitude and upstream blocking, appear fairly insensitive to the modified surface characteristics. Rather, the flow regime over

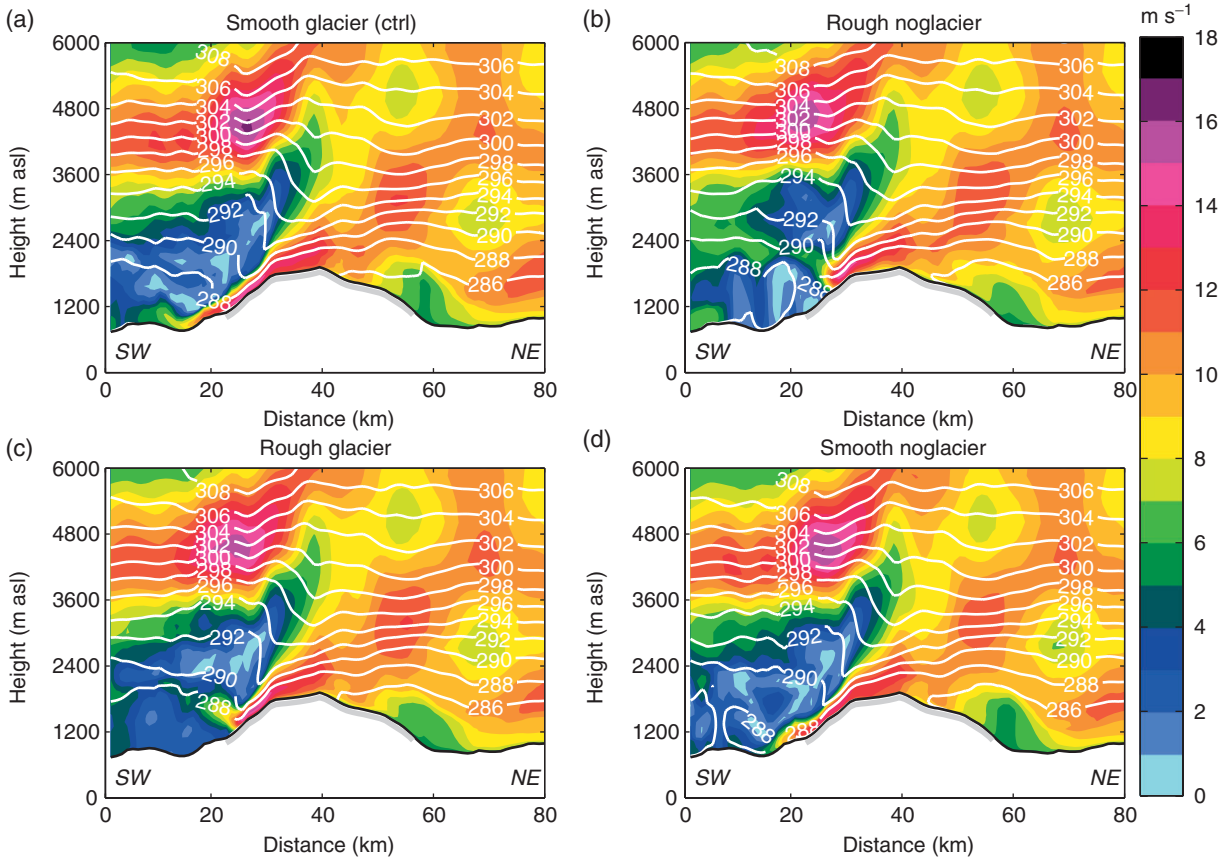

Figure 15. Vertical cross-section of simulated horizontal wind speed (shading, 1 m s^{-1} intervals) and potential temperature (2K intervals) over Hofsjökull at 1500 UTC on 13 August 2007 from the simulations: (a) smooth glacier (ctrl), (b) rough noglacier, (c) rough glacier and (d) smooth noglacier. The grey, solid line along the mountain surface indicates the location of the ice cap and thus the area affected by the land-use modifications. The location of the cross-section is indicated in Figure 4. The mean flow direction is from the right (northeast) to the left (southwest).

Hofsjökull and its temporal evolution are virtually the same in all four simulations and they appear to be governed by larger-scale diurnal variability in surface heat fluxes and/or synoptic forcings. Indeed, the flow regime's temporal evolution closely follows the pattern as predicted by the values of Nh/U (Smith, 1989) in all four simulation experiments. During daytime, Nh/U is close to 1, thus favouring wave amplification and even breaking. During night-time Nh/U increases, thus moving towards a regime more dominated by blocking with less prominent waves.

6. Discussion

In this study, we have systematically compared the effects of surface characteristics in terms of roughness and heat fluxes on mountain waves and associated downslope accelerated flow for typical summertime flow conditions over a mesoscale, ice-cap-covered mountain in central Iceland.

Unlike previous modelling studies in 2D (e.g. Richard *et al.*, 1989; Peng and Thompson, 2003; Vosper, 2004) and in 3D (e.g. Georgelin *et al.*, 1994; Ólafsson and Bougeault, 1997a), we find no clear damping effect of the surface roughness on the mountain lee-wave amplitude. In fact, we find strong lee waves for any of the two tested roughness lengths in our simulations. Furthermore, in daytime, we find signs of wave breaking. The latter finding stands in contrast to e.g. Ólafsson and Bougeault (1997a), who found that the introduction of surface roughness completely eliminated wave breaking for any tested Nh/U (0.5–4.5). On the other hand, Peng and Thompson (2003) did find wave breaking for sufficiently high values of Nh/U (1.95) with surface friction included in their 2D simulations. While the impact on the lee-wave amplitude from the surface roughness changes in our simulations is minimal, there is indeed an effect on the downslope accelerated flow, which is significantly reduced in speed and downslope penetration with an increased roughness length. The latter result is in line with studies such as Richard *et al.* (1989). One reason for the above-described discrepancies between our work and the aforementioned results may lie in the experimental set-up. While the earlier studies considered no-slip versus free-slip conditions and the surface roughness changes were applied to the entire model domains, our study considers only cases with non-zero surface roughness and we apply the surface changes only to a limited area.

Smith and Skyllingstad (2009) studied the impact of surface heat fluxes on downslope flows using 2D idealised simulations of flow over an isolated mountain. The ratio between the initial boundary-layer height (z_i = 200 m) and the mountain height (h = 400 m) in their simulations is close to that in our simulations during daytime. As in our simulations, no clear inversion was present in their simulations and the downslope accelerated flow was generated by IGW breaking. Their Nh/U of 1.2 was similar to the average Nh/U in our study. Smith and Skyllingstad (2009) found that strong surface heating (200 W m^{-2}) acted to significantly weaken the downslope flow and they found that a surface cooling of −50 W m^{-2} led to a strengthened downslope flow. Both experiments were compared to a simulation without any surface heat fluxes. In their strong heating case, they found convection to generate a deep mixed layer upstream of the mountain, which in turn prevented a strong mountain internal wave response. Furthermore, turbulent air from a mixed layer that grew above the mountain's height was advected downstream, thus acting to decelerate the downslope flow through diffusion. On the other hand, in our simulations the ABL height remains below the mountain-top level throughout the simulation and no such ABL air advection is seen. Also a surface cooling, which naturally increases the low-level air's stability and which Smith and Skyllingstad (2009) found to favour strong downslope winds, has no consistent impact on the downslope flow in our simulations. A reason for the disagreement between their results and ours could lie in the different spatial extent of the changes

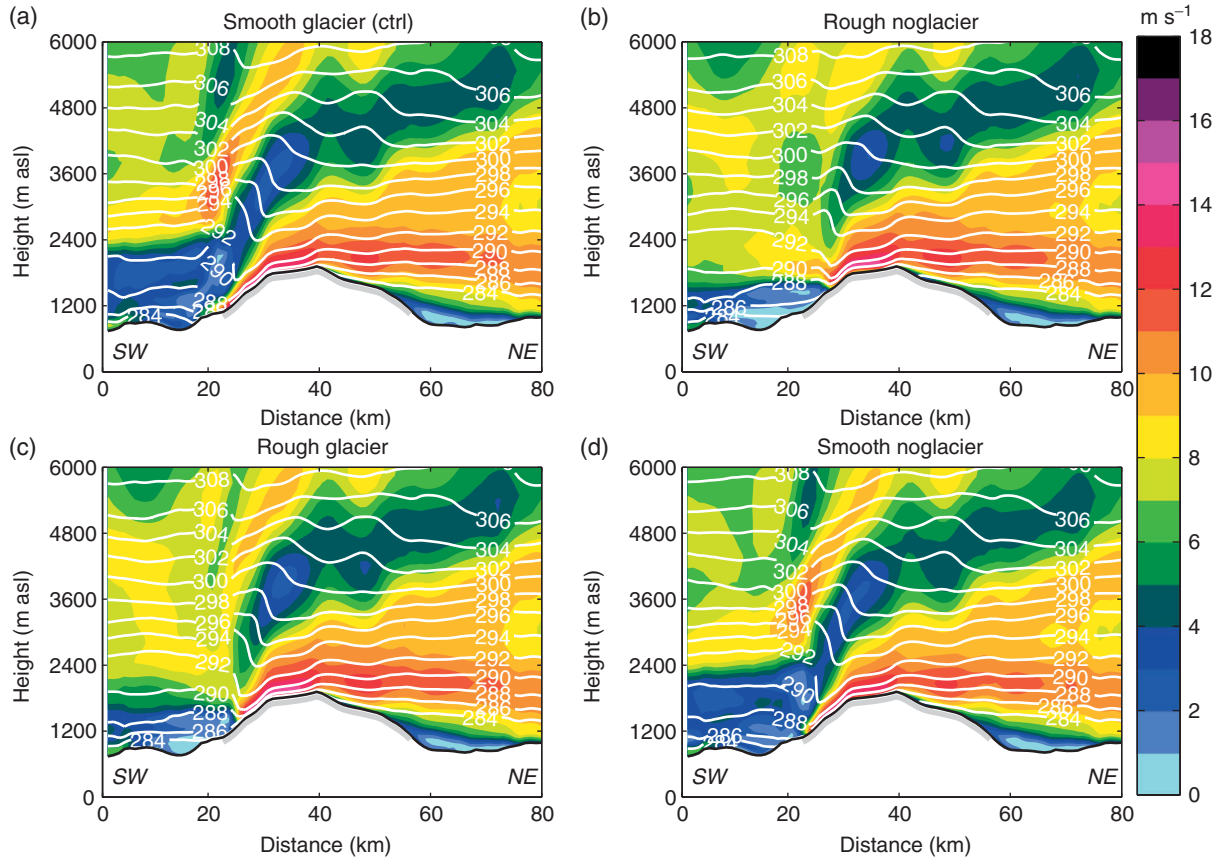

Figure 16. As Figure 15, but for 0300 UTC on 14 August 2007.

in the surface characteristics. The changes in the heat flux in our simulations apply only to the mountain surface, whereas Smith and Skyllingstad (2009) applied them to the whole model domain. Furthermore, the mountain width in their study ($a = 4000$ m) is only 1/10th of that in our study. Thus, Na/U was around 12 in their study, but between 38 and 66 in our study. This can be one of the reasons why their simulations contained rotors whereas ours do not.

Using idealised simulations of flow over an isolated mountain ridge, Jiang and Doyle (2008) also studied the effect of surface cooling and heating on downslope flow. They found that both surface cooling and indeed also surface heating led to an enhanced downslope flow. However, in their study the surface heat fluxes were changed only on the mountain's lee side. The large positive surface heat fluxes (300 W m^{-2}) in their simulations thus led to a further reduced low-level pressure on the lee side which in turn enhanced the downslope flow. In our simulations, the surface heat fluxes were changed on both sides of the mountain top and the results are therefore not directly comparable.

In contrast to several previous studies (e.g. Brinkmann, 1974; Jiang and Doyle, 2008; Valkonen *et al.*, 2010), we do not find any tendency for an increased downslope flow during night-time. The absence of a clear diurnal signal in the downslope flow acceleration in our study may depend on the values of Nh/U. In our study the Nh/U stays within a range of 1.1–1.6. In this range one would expect gravity waves and downslope accelerated flow to dominate (e.g. Smith, 1989). For larger diurnal variations in Nh/U, e.g. for different cases or locations, Nh/U may drop significantly below unity during daytime, leading to less or even no gravity wave activity and downslope accelerated flow. Consequently, we cannot exclude that there may be a diurnal signal in the downslope flow for the area investigated for other cases.

Previous studies have shown that elevated inversions can act to increase the frequency of (or for some situations even be necessary in the creation of) downslope accelerated flow (e.g. Vosper, 2004; Mobbs *et al.*, 2005; Smith and Skyllingstad, 2011). When an elevated inversion is present, the generation of downslope accelerated flow may be described as a transition from a subcritical to a supercritical flow, as described in shallow-water theory. We do not find a clear inversion in our case, but it is reasonable to assume that inversions do occur in the area of Hofsjökull and that shallow-water theory may apply in such cases. More case-studies and/or more detailed studies of climate simulations could shed some light on both the diurnal signal in downslope flows over Hofsjökull and on the importance of inversions in the creation of the climatologically prominent downslope flow over Hofsjökull.

Katabatic winds may also be a factor that modifies the surface flow over Hofsjökull. In their study of observations from FLOHOF, Reuder *et al.* (2012) found that the heating of the surface surrounding the Hofsjökull glacier leads to katabatic winds that reach typically a maximum of 4–6 m s^{-1} at the edge of the glacier. These winds blow away from the glacier in all directions directed towards lower altitude and consequently they contribute to increasing the downslope winds and reducing the upstream winds. It is difficult to estimate the katabatic contribution to the total flow in our study. However, the fact that there is no consistent difference in wind speed between the 'glacier' and 'noglacier' experiments would indicate no such significant contribution. The results of Smith and Skyllingstad (2011) would also speak against a significant contribution to the downslope accelerated flow from katabatic winds. They found the presence of a strong low-level inversion to be a requirement for such a contribution, and we do not have a strong low-level inversion in our simulations.

For future case-studies of real flow over Hofsjökull, and indeed other mountains also, upstream profiles from a boundary-layer profiler or an RPAS like the SUMO system would be desirable. This would allow for a better classification of the upstream flow and it would also enable a better assessment of the model input boundary conditions. More AWSs would also be desirable, especially downstream to allow for a better observational mapping of the horizontal extent of the downslope flow.

7. Summary and conclusions

Recent dynamical downscaling of flow over Iceland indicates prominent downslope winds over the larger ice caps. In this study, our main goal has been to investigate the impact of the ice cap's smooth and cold surface on this flow pattern. Both surface properties have previously been found to enhance mountain waves and downslope winds.

Through a series of numerical sensitivity experiments using the WRF model, we have investigated the flow over the mesoscale-sized, ice-cap-covered Hofsjökull mountain in central Iceland. In the investigations we have focused on a real flow case from the FLOHOF campaign, in summer 2007. We find that the ice cap's low surface roughness contributes to an increase in the downslope wind's strength and horizontal extent, while its relatively low surface temperature has no consistent impact in this regard. Neither the changes in surface roughness, nor the changes in surface temperatures have any significant impact on the lee-wave amplitude, and larger-scale diurnal variability and/or synoptic flow conditions dominate the temporal variability in the flow regime.

The results from the present study are relevant both for the understanding of factors affecting downslope acceleration of stably stratified flow and because the glaciers are diminishing in response to a warming climate.

Acknowledgements

We would like to express our gratitude to two anonymous reviewers whose comments significantly improved the manuscript. We would also like to thank all participants of FLOHOF, especially Joachim Reuder, Stephanie Mayer, Martin Müller, Pascal Brisset and Christian Lindenberg.

References

Ágústsson H, Ólafsson H. 2012. The bimodal downslope windstorms at Kvísker. *Meteorol. Atmos. Phys.* **116**: 27–42.

Brinkmann WAR. 1974. Strong downslope winds at Boulder, Colorado. *Mon. Weather Rev.* **102**: 592–602.

Chen F, Dudhia J. 2001. Coupling an advanced land surface-hydrology model with the Penn State-NCAR MM5 modeling system. Part 1. Model implementation and sensitivity. *Mon. Weather Rev.* **129**: 569–585.

Chen WD, Smith RB. 1987. Blocking and deflection of airflow by the Alps. *Mon. Weather Rev.* **115**: 2578–2597.

Dudhia J. 1989. Numerical study of convection observed during the winter monsoon experiment using a mesoscale two-dimensional model. *J. Atmos. Sci.* **46**: 3077–3107.

Epifanio CC, Qian T. 2008. Wave–turbulence interactions in a breaking mountain wave. *J. Atmos. Sci.* **65**: 3139–3158.

Georgelin M, Richard E, Petitdidier M, Druilhet A. 1994. Impact of subgrid-scale orography parameterization on the simulation of orographic flows. *Mon. Weather Rev.* **122**: 1509–1522.

Gill AE. 1982. *Atmosphere–Ocean Dynamics*. Academic Press: London.

Hong S, Dudhia J, Chen S. 2004. A revised approach to ice microphysical processes for the bulk parameterization of clouds and precipitation. *Mon. Weather Rev.* **132**: 103–120.

Janjić ZI. 1994. The step-mountain eta coordinate model: Further development of the convection, viscous sublayer, and turbulent closure schemes. *Mon. Weather Rev.* **122**: 927–945.

Janjić ZI. 2001. 'Nonsingular Implementation of the Mellor–Yamada Level 2.5 Scheme in the NCEP Meso Model'. NOAA/NWS/NCEP Office Note 437. NCEP Environmental Modeling Center: Camp Springs, MD.

Jiang Q, Doyle JD. 2008. On the diurnal variation of mountain waves. *J. Atmos. Sci.* **65**: 1360–1377.

Kilpeläinen T, Vihma T, Ólafsson H. 2011. Modelling of spatial variability and topographic effects over Arctic fjords in Svalbard. *Weather and Forecasting* **63A**: 223–237.

Lane TP, Doyle JD, Sharman RD, Shapiro MA, Watson CD. 2009. Statistics and dynamics of aircraft encounters of turbulence over Greenland. *Mon. Weather Rev.* **137**: 2687–2702.

Lilly DK. 1972. Wave momentum flux –A GARP problem. *Bull. Am. Meteorol. Soc.* **53**: 17–23.

Mayer S, Sandvik A, Jonassen MO, Reuder J. 2012. Atmospheric profiling with the UAS SUMO: A new perspective for the evaluation of fine-scale atmospheric models. *Meteorol. Atmos. Phys.* **116**: 15–26, doi: 10.1007/s00703-010-0063-2.

Mayer S, Hattenberger G, Brisset P, Jonassen MO, Reuder J. 2012. A 'no-flow-sensor' wind estimation algorithm for unmanned aerial systems. *Int. J. Micro Air Vehicles* **4**: 15–29.

Mayer S, Jonassen MO, Sandvik A, Reuder J. 2012. Profiling the Arctic stable boundary layer in Advent Valley, Svalbard: Measurements and simulations. *Boundary-Layer Meteorol.* **143**: 507–526.

Mellor GL, Yamada T. 1982. Development of a turbulence closure model for geophysical fluid problems. *Rev. Geophys. Space Phys.* **20**: 851–875.

Mlawer EJ, Taubman SJ, Brown PD, Iacono MJ, Clough SA. 1997. Radiative transfer for inhomogeneous atmospheres: RRTM, a validated correlated-k model for the longwave. *J. Geophys. Res.* **102**: 16663–16682, doi: 10.1029/97JD00237.

Mobbs SD, Vosper SB, Sheridan PF, Cardoso R, Burton RR, Arnold SJ, Hill MK, Horlacher V, Gadian AM. 2005. Observations of downslope winds and rotors in the Falkland Islands. *Q. J. R. Meteorol. Soc.* **131**: 329–351.

Ólafsson H, Bougeault P. 1997a. The effect of rotation and surface friction on orographic drag. *J. Atmos. Sci.* **54**: 193–210.

Ólafsson H, Bougeault P. 1997b. Why was there no wave breaking in PYREX? *Beitr. Phys. Atmos.* **70**: 167–170.

Ólafsson H, Ágústsson H. 2009. Gravity wave breaking in easterly flow over Greenland and associated low-level barrier and reverse tip-jets. *Meteorol. Atmos. Phys.* **104**: 191–197.

Peng MS, Thompson WT. 2003. Some aspects of the effect of surface friction on flows over mountains. *Q. J. R. Meteorol. Soc.* **129**: 2527–2557.

Raymond DJ. 1972. Calculation of airflow over an arbritrary ridge including diabatic heating and cooling. *J. Atmos. Sci.* **29**: 837–843.

Reuder J, Brisset P, Jonassen MO, Müller M, Mayer S. 2009. The Small Unmanned Meteorological Observer SUMO: A new tool for atmospheric boundary-layer research. *Meteorol. Z.* **18**: 141–147.

Reuder J, Ablinger M, Ágústsson H, Brisset P, Brynjólfsson S, Garhammer M, Jóhannesson T, Jonassen M, Kühnel R, de Lange T, Lindenberg C, Malardel S, Mayer S, Müller M, Ólafsson H, Rögnvaldsson O, Schäper W, Spengler T, Zängl G, Egger J. 2012. FLOHOF 2007: An overview of the mesoscale meteorological field campaign at Hofsjökull, Central Iceland. *Meteorol. Atmos. Phys.* **116**: 1–13, doi: 10.1007/s00703–010–0118–4.

Richard E, Mascart P, Nickerson EC. 1989. The role of surface friction in downslope windstorms. *J. Appl. Meteorol.* **28**: 241–251.

Rögnvaldsson O, Ágústsson H, Einarsson EM, Ólafsson H, Björnsson H, Sveinsson OGB. 2007. 'Status report for year one of the RÁV project' (in Icelandic). http://thjarkur.belgingur.is/wordpress/wp-content/uploads/RAVarsskyrsla2007.pdf (accessed 7 January 2014).

Skamarock WC, Klemp JB, Dudhia J, Gill DO, Barker DM, Duda MG, Huang XY, Wang W, Powers JG. 2008. 'A description of the advanced research WRF version 3', Technical Note TN-475+STR. NCAR: Boulder, CO.

Smeets CJPP, van den Broeke MR. 2008. Temporal and spatial variations of the aerodynamic roughness length in the ablation zone of the Greenland Ice Sheet. *Boundary-Layer Meteorol.* **128**: 315–338.

Smith RB. 1989. Hydrostatic airflow over mountains. *Adv. Geophys.* **31**: 59–81.

Smith RB, Grønås S. 1993. Stagnation points and bifurcation in 3D mountain flow. *Tellus* **45A** 28–43.

Smith CM, Skyllingstad ED. 2009. Investigation of upstream boundary-layer influence on mountain wave breaking and lee wave rotors using a large-eddy simulation. *J. Atmos. Sci.* **66**: 3147–3164.

Smith CM, Skyllingstad ED. 2011. Effects of inversion height and surface heat flux on downslope windstorms. *Mon. Weather Rev.* **139**: 3750–3764.

Stewart RE, Bachand D, Dunkley RR, Giles AC, Lawson B, Legal L, Miller ST, Murphy BP, Parker MN, Paruk BJ, Yau MK. 2005. Winter storms over Canada. *Atmos. Ocean* **131**: 223–247.

Stull RB. 1988. *An Introduction to Boundary-Layer Meteorology*. Springer: Berlin.

Valkonen T, Vihma T, Kirkwood S, Johansson MM. 2010. Fine-scale model simulations of gravity waves generated by Basen nunatak in Antarctica. *Tellus* **62A** 319–332.

Vosper SB. 2004. Inversion effects on mountain lee waves. *Q. J. R. Meteorol. Soc.* **130**: 1723–1748.

Wahr MJ, Oort AH. 1984. Friction- and mountain-torque estimates from global atmospheric data. *J. Atmos. Sci.* **41**: 190–204.

